Environmental Science and Pollution Research
https://doi.org/10.1007/s11356-019-06872-7

RESEARCH ARTICLE

Zinc toxicity alters the photosynthetic response of red alga *Pyropia yezoensis* to ocean acidification

Jing Ma[1] · Wen Wang[1] · Xiaoyan Liu[1] · Zhiqin Wang[1] · Guang Gao[1] · Hailong Wu[1] · Xinshu Li[1] · Juntian Xu[1,2,3]

Received: 21 February 2019 / Accepted: 23 October 2019

Abstract

The globally changing environmental climate, ocean acidification, and heavy metal pollution are of increasing concern. However, studies investigating the combined effects of ocean acidification and zinc (Zn) exposure on macroalgae are very scarce. In this study, the photosynthetic performance of the red alga *Pyropia yezoensis* was examined under three different concentrations of Zn (control, 25 (medium), and 100 (high) μg L^{-1}) and pCO_2 (400 (ambient) and 1000 (high) μatm). The results showed that higher Zn concentrations resulted in increased toxicity for *P. yezoensis*, while ocean acidification alleviated this negative effect. Ocean acidification increased the relative growth rate of thalli under both medium and high Zn concentrations. The net photosynthetic rate and respiratory rate of thalli also significantly increased in response under ocean acidification, when thalli were cultured under both medium and high Zn concentrations. Malondialdehyde levels decreased under ocean acidification, compared to ambient CO_2 conditions and either medium or high Zn concentrations. The activity of superoxide dismutase increased in response to high Zn concentrations, which was particularly apparent at high Zn concentration and ocean acidification. Immunoblotting tests showed that ocean acidification increased D1 removal, with increasing expression levels of the PSII reaction center proteins D2, CP47, and RbcL. These results suggested that ocean acidification could alleviate the damage caused by Zn exposure, thus providing a theoretical basis for a better prediction of the impact of global climate change and heavy metal contamination on marine primary productivity in the form of seaweeds.

Keywords High CO_2 · Photosynthesis · *Pyropia yezoensis* · Zn

Introduction

Due to anthropogenic activities, the CO_2 in the atmosphere has been predicted to increase from 400 to about 1000 ppm by 2100 (Stoneman and Smith 2012), with the potential to reach 2000 ppm by 2300 (Caldeira and Wickett 2003). Atmospheric CO_2 dissolves in seawater, where it forms carbonic acid, which is unstable and dissociates into hydrogen ions (H^+), bicarbonate ions (HCO_3^-), and a small amount of carbonate ions (CO_3^{2-}). The increasing H^+ concentration in seawater leads to a pH decrease, which has been named ocean acidification (Brierley and Kingsford 2009; Landschützer et al. 2018). This ocean acidification has been predicted to result in a pH decrease of 0.14–0.41 units by 2100 and 0.3–0.7 units by 2300 and induced changes in the marine ecosystems (Doney 2009). Heavy metals found in marine environments which originate from both anthropogenic and natural sources also contribute significantly to the overall acidification threat in some coastal regions (Cai et al. 2011); for metals such as cadmium (Cd), lead (Pb), zinc (Zn), nickel (Ni), and copper

Responsible editor: Robert Duran

Electronic supplementary material The online version of this article (https://doi.org/10.1007/s11356-019-06872-7) contains supplementary material, which is available to authorized users.

✉ Juntian Xu
jtxu@jou.edu.cn

[1] Jiangsu Key Laboratory of Marine Bioresources and Environment, Jiangsu Ocean University, No. 59 Cangwu Road, Lianyungang 222005, Jiangsu, People's Republic of China

[2] Jiangsu Key Laboratory of Marine Biotechnology, Jiangsu Ocean University, No. 59 Cangwu Road, Lianyungang 222005, Jiangsu, People's Republic of China

[3] Co-Innovation Center of Jiangsu Marine Bio-industry Technology, No. 59 Cangwu Road, Lianyungang 222005, Jiangsu, People's Republic of China

Published online: 14 December 2019

(Cu), anthropogenic emissions significantly exceed natural inputs (Clark et al. 2002).

Calcifying and non-calcifying macroalgae will respond differently to ocean acidification. Calcium carbonate saturation would decrease calcification and impact structure formation of crustose coralline algae (Webster et al. 2013). Due to the different effects of ocean acidification and CO_2 concentration, the increase in dissolved inorganic carbon and ocean acidification either positively or negatively affects non-calcifying algae (Hepburn et al. 2011; Cornwall et al. 2012; Gao et al. 2017). Kuffner et al. (2008) reported that the recruitment rate and growth of crustose coralline algae were severely inhibited in the elevated CO_2 mesocosms. Gattuso et al. (1997) found that there was a slight net dissolution of $CaCO_3$ (0.8 mmol m^{-2} day^{-1}) on a fringing reef at Moorea under high CO_2 condition. Researches also revealed that ocean acidification had decreased the calcification rate of scleractinian corals and other reef-building organisms (Gattuso et al. 1997; Leclercq et al. 2002), while non-calcifying algae had different response to ocean acidification. High CO_2 concentration had enhanced the photosynthesis of intertidal macroalgae (Zou and Gao 2005) and increased the growth of red algae *Prophyra yezoensis* (Gao et al. 1991). Decreased growth rates were found under high CO_2 level in *Gracilaria tenuistipitata* (García-Sánchez et al. 1994).

Ocean acidification and heavy metal pollution often occur simultaneously, especially in coastal areas (Stewart et al. 2016). The decreased pH of marine water results in lower OH^- and CO_3^{2-} concentrations, and decreasing their concentrations increases the concentrations of metal ions (Millero et al. 2009). OH^- and CO_3^{2-} form complexes with divalent or trivalent metal ions, thus affecting their solubility, adsorption, toxicity, and redox rate in marine water. This had been reported to cause further increases of the concentration of free heavy metals in the marine water in response to heavy metal pollution (Millero et al. 2009). Furthermore, it was reported that high CO_2 concentration could increase the growth inhibition of *Chlorella vulgaris* cells by TiO_2NPs exceeding 5 mg L^{-1} (Sadiq et al. 2011). Leal et al. (2018) evaluated the meiospore development of the kelps *Macrocystis pyrifera* and *Undaria pinnatifida* exposed to the current pH levels and those predicted for 2100 (8.16 and 7.65, respectively), temperature (12 and 16 °C, respectively), and two Cu concentrations (without Cu and species-specific germination Cu-EC50). The result showed that in response to ocean acidification and ambient temperature/ocean acidification conditions, irrespective of copper exposure, the meiospore germination of both species decreased by 5–18%. The germling growth rate and gametophyte development were inhibited under Cu-EC50 exposure, compared to without Cu treatment. To date, research on the coupled effect of ocean acidification and the exposure to heavy metals is limited (Franklin et al. 2000; Gao et al. 2017; Leal et al. 2018) and the photosynthetic characteristics and protective mechanisms of macroalgae are yet to be comprehensively studied.

Heavy metals are the most common types of coastal contaminants (Doney 2009). Several metals (such as Cu and Zn) are essential cofactors for a number of biochemical processes (e.g., photosynthesis, synthesis of the D1 protein in PSII, and antioxidant system) (Gao et al. 2017; Mousavi et al. 2012). However, at elevated concentrations, all heavy metals are toxic to biological organisms, even those with essential functions. Zn plays an important role in enzymes related to photosynthesis and metabolic function, such as carbonic anhydrase, acid phosphatase, and alkaline phosphatase. Zn can be absorbed by algae, which leads to an increase of the growth of their thalli (Boyer and Brand 1998; Gao et al. 2009). Once the algae are contaminated with Zn or have absorbed excess Zn, toxic effects will impact their growth and generated reactive oxygen species (ROS) in the thalli.

ROS damage the cell membrane and generates a large amount of malondialdehyde (MDA) which is a biomarker for cumulative peroxidation damage in membrane lipids in response to heavy metal exposure. It functions as a degradation product of n-3 polyunsaturated fatty acids (PUFAs) in membranes and stimulates the oxidative stress reaction of algae (Nanda and Agrawal 2016). The production of antioxidants with low molecular weight (e.g., ascorbic acid (AsA), glutathione peroxidase (GSH), and non-protein thiol (NPT)) and antioxidant enzymes (e.g., SOD, ascorbate peroxidase (APX), guiacol peroxidase (GPX), and CAT) will be enhanced (Singh et al. 2006). These changes are important to prevent plant oxidative stress by increasing the activity of one or more enzymes in response to Zn stress (Yang et al. 2016). Destruction of the antioxidant enzyme system will affect both the growth and physiology of the algae and can even lead to their death (Volland et al. 2014; Cai et al. 2019). However, Zn has been reported to ameliorate the toxicity and uptake of Cr in plant cells (Mallick et al. 2010; Branzini et al. 2012). In addition, high concentrations of Zn can change the permeability of the cell membrane, which causes cellular morphological variation (Leusch et al. 1995). No significant difference was found in the growth or reproduction of *Karenia mikimotoi* in response to exposure to Zn levels between 1 and 5 mg L^{-1}, while the growth of cells was inhibited by a concentration > 10 mg L^{-1} Zn (Cai et al. 2019). Omar (2002) reported that when *Scendesmus obliquus* was treated with 7.93 μg L^{-1} and 24.83 μg L^{-1} Zn, biomass decreased by 19% and 54%, respectively. Lv et al. (2017) found that the specific growth rates of *Sargassum muticum* and *Gracilaria chouae* decreased under exposure to a Zn level of 1 mg L^{-1} after cultivation for 3 days.

Porphyra species are edible and therefore widely cultivated in Southeast and East Asian countries (e.g., China, Korea, and Japan) (Gao et al. 2019). In China, *Pyropia yezoensis* is mainly cultivated in Shandong, Jiangsu, and Zhejiang provinces

(Ma and Cai 1996). Researches reported that *P. yezoensis* could utilize HCO_3^- by CO_2 concentrating mechanisms (CCMs) to improve algal performance under resource-limiting conditions (Gao et al. 2012; Li et al. 2016; Gao et al. 2017; Qu et al. 2017). In this study, *P. yezoensis* was selected to investigate the coupling effect of ocean acidification and Zn exposure, and it was hypothesized that the response of *P. yezoensis* to Zn is pCO_2-dependent. Increasing the pCO_2 was further hypothesized to alleviate Zn toxicity. To test this hypothesis, the algal growth rate, pigment content, photosynthesis rate, and the protein expression level of photosystem II were monitored (Fig. 1). These data were used to analyze the response of *P. yezoensis* to ocean acidification and its adaptation mechanisms.

Material and methods

Thalli collection and culture conditions

P. yezoensis was collected from the intertidal zone of Gaogong island (119.30° E, 34.50° N), Lianyungang, China, and transported to the laboratory on ice. Selected thalli were cleaned with filtered natural seawater to remove both debris and surface epiphytes. Well-grown thalli were selected for preculture in aquaculture tanks, containing 1 L filtered sterile seawater, enriched with 60 μM $NaNO_3$ and 8 μM KH_2PO_4. The light intensity was maintained at 160 μmol photons m^{-2} s^{-1}, at a 12:12-h light/dark cycle, and the temperature was controlled at 10 °C (± < 0.5 °C), which is the same level as the sampling area, until algae were required for experiments. Three triplicates were conducted per treatment.

After preincubation, selected thalli (length of ~ 1 cm) were cultured in 500-mL polycarbonate flasks, with six thalli per flask. Cultures were maintained under three Zn concentrations (control, LZn; 25 μg L^{-1}, MZn; 100 μg L^{-1}, HZn) for 1 week under either ambient (400 μatm, LC) or high (1000 μatm, HC) pCO_2 levels. Zn (0.5 μg L^{-1}) in natural seawater without added $ZnSO_4$ was applied as control (LZn). Zn concentrations were selected according to Chakraborty and Owens (2015). They were measured by inductively coupled plasma atomic emission spectrometry (ICP-AES) (iCAP6300, Thermo fisher, USA). The procedures used for Zn tests conformed to protocols for the reduction of the risk of metal contamination (Leal et al. 2016). The elevated pCO_2 level were selected as representation of the predicted levels by the year 2100, based on the representative concentration pathway (RCP) 8.5 (Gattuso et al. 2015; Gao et al. 2018a, 2018b). The 400 μatm CO_2 concentration was achieved by bubbling ambient air through the medium. And the high CO_2 concentration was achieved via bubbling of enriched CO_2 from a CO_2 plant incubator (HP1000G-D, Ruihua Instruments, Wuhan, China). The pH levels in LC and HC cultures were maintained at 8.18 and 7.83, respectively, with variations of < 0.05, as measured by a pH meter on the NBS scale after each seawater medium change (pH 700, Eutech Instruments, Singapore). The culture conditions were consistent with the preincubation conditions as described above, and the seawater medium was changed every 2 days. All experiments were conducted in the same light incubator (GXZ-500C, Ningbo, China). After culture for 6 days, all thalli were used to measure the relative growth rate (RGR) and randomly selected algae were used to measure different parameters. Each treatment was performed in triplicate (Fig. 1).

Measurement of *P. yezoensis* growth

The growth of *P. yezoensis* was measured by weighing the fresh thalli in each flask. Absorbent paper was used to remove surface water from thalli before weighing. The RGR was calculated according to Eq. (1):

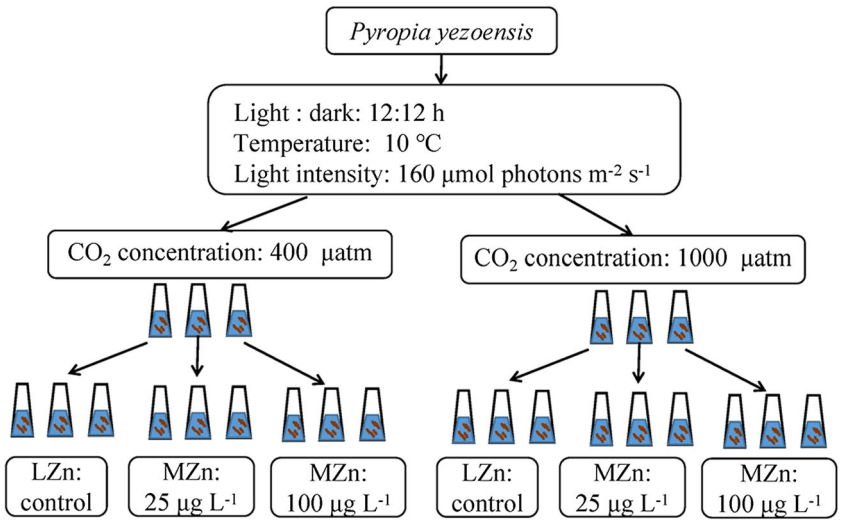

Fig. 1 Graphic scheme of the experimental design in which *P. yezoensis* were cultured at a 12:12 h light/dark cycle, and where the light intensity (160 μmol photons m^{-2} s^{-1}) and the temperature (10 ± < 0.5 °C) was controlled for 1 week under different Zn (LZn, control; MZn, 25 μg L^{-1} Zn; HZn, 100 μg L^{-1} Zn) and CO_2 concentrations (LC, 400 μatm CO_2; HC, 1000 μatm CO_2) (see detailed description in the "Material and methods" section)

$$\mathrm{RGR} = 100 \times (\ln W_t - \ln W_0)/t \quad (1)$$

where W_0 represents the initial fresh weight and W_t represents the fresh weight after t number of days. The total fresh weight of thalli cultured at different Zn levels for 6 days was measured to determine the EC50 value, which is defined as the heavy metal concentration that caused a 50% inhibition in growth of experimental thalli compared to controls (Mamboya et al. 2009). The EC50 was determined by using the regression line, which was plotted by the least-square method, using three replicates of growth rate as discrete data points (Haglund et al. 1996).

Chlorophyll fluorescence measurements

After 10 min of dark adaptation, randomly selected thalli segments were used to measure the chlorophyll fluorescence using a portable fluorometer (Dual-PAM, Walz, Germany). The saturating pulse was set to 5000 μmol photons m^{-2} s^{-1} (0.8 s), and experiments were performed in triplicate. The relative electron transfer rate (rETR) was calculated according to Eq. (2) (Genty et al. 1989):

$$\mathrm{rETR}\left(\mu\mathrm{mol}\ e^{-1}\ m^{-2}\ s^{-1}\right) = \mathrm{Fv'/Fm'} \times 0.5 \times \mathrm{PFD} \quad (2)$$

where Fv'/Fm' represents the effective PSII quantum yield and PFD represents the photosynthetically active photo flux density. rETR rapid light curves were acquired from seven varying levels of photosynthetically active radiation (PAR) intensity (every light step was measured for 10 s, and the period of the light curve lasted for ~ 70 s). The maximum rETR ($\mathrm{rETR_{max}}$), efficiency of electron transport (α), and saturating irradiance (I_k) were established from the rETR curve and were calculated according to Eqs. (3–5) as follows (Eilers and Peeters 1988):

$$\mathrm{rETR} = I/\left(\alpha \times I^2 + b \times I + c\right) \quad (3)$$

$$\mathrm{rETR_{max}} = 1/\left[b + 2 \times (a \times c)^{1/2}\right] \quad (4)$$

$$I_k = (c/\alpha)^{1/2} \quad (5)$$

where I represents the incident irradiance; a, b, and c represent the adjustment parameters; and α represents $1/c$. The parameter "a" is regarded as the photoinhibition term and can also be considered as a function of the exposure time above I_k, according to the modification description (Eilers and Peeters 1988; Macedo et al. 2002).

Photosynthesis and respiration rate measurements

The net photosynthetic rate and respiration rate of algae were measured using a Clark-type oxygen electrode (YSI Model 5300A, USA) following to the method reported by Gao et al. (2017). The experiment was conducted from 10:00 a.m. to 13:00 p.m. Thalli were cut into segments of about 1 cm and placed under the aforementioned culture conditions for 1 h to avoid effects of stress response following cutting. Then, 0.02 g of fresh thalli segments were randomly selected and transferred to a photosynthetic chamber containing 8 mL of culture seawater inside each algae culture flask. The medium was constantly stirred. The temperature was controlled at 10 °C, and irradiance conditions were maintained at 160 μmol photons m^{-2} s^{-1}. The measurement was finished within 5 min, during which, the pH did not vary. The respiration rate was measured after 2 min of dark adaptation, and the same method was used that was used to measure photosynthesis (Xu and Gao 2012; Gao et al. 2017).

Pigment concentration analysis

Approximately 0.02 g of fresh thalli was extracted in 5 mL of anhydrous methanol at 4 °C for 24 h, in the dark. The absorbances of samples were measured at 666 nm and 652 nm using an ultraviolet/visible (UV/vis) spectrophotometer (Ultrospect 3300 pro, Amersham Bioscience, Sweden). The chlorophyll a content (Chl a) was calculated as follows according to Porra et al. (1989).

$$\mathrm{Chl}\ a = 16.29 \times \mathrm{A665.2} - 8.54 \times \mathrm{A652.0} \quad (6)$$

Malondialdehyde content and activity of superoxide dismutase

MDA concentrations were used as an indicator of the level of lipid peroxidation (Ma et al. 2016) and were measured using MDA assay kits (Jiancheng, Nanjing, Jiangsu, China). Thalli (0.1 g) were sampled from each treatment and were homogenized in 0.9 mL extraction buffer, using a pestle and mortar. The homogenates were centrifuged at 3500g for 15 min at 4 °C, and supernatants were collected and analyzed using a microplate reader (Multiskan FC, Thermo, Shanghai, China) to determine MDA concentrations at 532 nm, according to the manufacturer's instructions. The MDA concentration is expressed in mmol g^{-1} fresh weight (FW).

SOD activity was measured according to Jiang and Prognon (2006). Using pestle and mortar, 0.1 g of each sample was homogenized in 0.9 mL phosphate buffer. Homogenates were centrifuged at 3500g for 10 min at 4 °C, and the supernatant was collected for the measurement of SOD activity. Samples were measured at an absorbance of 450 nm using a microplate reader (Multiskan FC, Thermo, Shanghai, China). SOD activity was assessed as activity units per gram (FW).

Protein concentration measurement by immunoblotting

Algal thylakoid membrane proteins were extracted in cool extracting medium (50 mM Tris–HCl, pH 7.6, 5.0 mM $MgCl_2$, 10 mM NaCl, 0.4 M sucrose, and 0.1% BSA) according to the method reported by Ma et al. (2016). Protein concentrations were determined using a microplate reader (Multiskan FC, Thermo, Shanghai, China) and compared to a bovine serum albumin (BSA) standard as reference. Extracted proteins were mixed with 5× loading buffer (Shenggong, Shanghai, China), and the mixture was boiled for 5 min. Two micrograms of Chl per spot was used for 12% sodium dodecyl sulfate-polyacrylamide gel electrophoresis (SDS-PAGE). The gel was then transferred to a PVDF membrane and immunoblotted with antibodies (RbcL, D1, D2, and CP47; Agrisera). Antibodies were detected with a chemiluminescence detection system (Tanon 5500, Shanghai, China), following the manufacturer's instructions.

Data analysis

Results are expressed as mean values ± standard deviation. The effects of ocean acidification and Zn concentrations on RGR, net photosynthetic rate, respiration rate, Chl *a*, MDA, and SOD were analyzed by two-way analysis of variance (ANOVA). One-way ANOVA was conducted to analyze each parameter under the same CO_2 concentration at different Zn conditions. EC50 values were analyzed by the nonlinear curve fit of Origin 9.0. Tukey's HSD analysis was conducted for post hoc investigation. Origin 9.0 software was used to perform statistical analysis. A 95% confidence interval was set for all tests.

Results

RGR

Two-way ANOVA results showed that CO_2 and Zn had an interactive effect ($p < 0.001$), and Zn concentration exerted a dominant effect on the RGR of *P. yezoensis* ($p < 0.001$). This suggests that the effects of Zn concentration on the RGR varied between ambient and high CO_2 concentrations (Table S1). The RGR significantly decreased from 29.90 ± 0.59% with LZn exposure to 21.61 ± 1.52% with HZn exposure ($p = 0.000$), under ambient CO_2 concentrations. At high CO_2 concentrations, the RGR also significantly decreased from 31.95 ± 1.16% (control) to 28.06 ± 1.10% ($p = 0.004$) and 26.96 ± 1.15% ($p = 0.001$) in MZn and HZn treatments, respectively. RGRs were significantly increased by elevated CO_2 concentrations under MZn or HZn conditions, compared to ambient CO_2 concentrations ($p < 0.05$) (Fig. 2). Significant differences were observed under both MZn and HZn treatments, compared to controls ($p < 0.05$). Nonlinear curve fitting established the EC50 values as 54.54 ± 3.44 μg L^{-1} and 57.22 ± 5.83 μg L^{-1} Zn under ambient and high CO_2 concentrations, respectively. No significant differences were found between EC50 under ambient and high CO_2 level ($p > 0.05$) (Table 1).

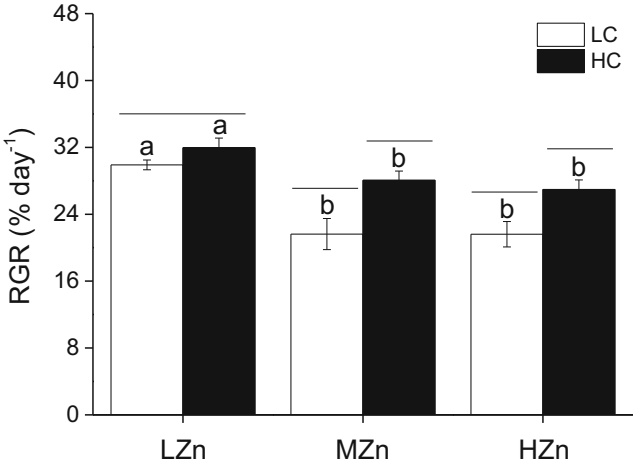

Fig. 2 Relative growth rate of *P. yezoensis* cultured under different Zn and CO_2 concentrations. LZn, control; MZn, 25 μg L^{-1} Zn; HZn, 100 μg L^{-1} Zn; LC, 400 μatm CO_2; HC, 1000 μatm CO_2. Error bars indicate the standard deviation ($n = 3$). Horizontal lines represent significant differences ($p < 0.05$) between ambient and elevated CO_2 levels at the same Zn concentration. Different letters represent significant differences ($p < 0.05$) at different Zn concentrations and the same CO_2 concentration

Fluorescence parameters

Fluorescence parameters were acquired from the rETR-irradiance curves and were used to establish the $rETR_{max}$, α, and I_k (Fig. S1, Table 2). Zn and CO_2 exerted interactive effects on $rETR_{max}$ ($p < 0.001$), while Zn exerted a dominant effect ($p < 0.001$) (Table S2). Under ambient CO_2 concentrations, MZn and HZn increased the $rETR_{max}$ to 74.2 ± 8.57 μmol e^{-1} m^{-2} s^{-1} ($p = 0.007$) and 56.01 ± 4.31 μmol e^{-1} m^{-2} s^{-1} ($p = 0.523$), respectively, compared to that at LZn. Under high CO_2 concentrations, $rETR_{max}$ increased from 61.44 ± 5.94 μmol e^{-1} m^{-2} s^{-1} (LZn) to 76.02 ± 5.66 μmol e^{-1} m^{-2} s^{-1} (MZn) ($p = 0.013$), and then decreased to 57.15 ± 3.26 μmol e^{-1} m^{-2} s^{-1} (HZn) ($p = 0.342$). No significant

Table 1 The EC50 value of *P. yezoensis* cultured at different Zn concentrations and CO_2 concentrations. LZn, control; MZn, 25 μg L^{-1}; HZn, 100 μg L^{-1}; LC, 400 μatm; HC, 1000 μatm

	EC50 (μg L^{-1})
LC	54.54 ± 3.44 [a]
HC	57.22 ± 5.83 [a]

Data are the means ± SD ($n = 3$). Different letters represent the significant difference ($p < 0.05$) among the Zn concentrations at the same CO_2 concentration

Table 2 The maximum rETR ($rETR_{max}$), electron transport efficiency (α), and saturating irradiance (I_k) of *P. yezoensis* cultured at different Zn concentrations and CO_2 concentrations. LZn, control; MZn, 25 μg L^{-1}; HZn, 100 μg L^{-1}; LC, 400 μatm; HC, 1000 μatm

	$rETR_{max}$ (μmol e^{-1} m^{-2} s^{-1})	α	I_k (μmol photons m^{-2} s^{-1})
LC-LZn	52.38 ± 6.05 a	0.14 ± 0.01 a	367.87 ± 31.62 ab
LC-MZn	74.2 ± 8.57 b	0.16 ± 0.00 a	475.42 ± 61.43 ab
LC-HZn	56.01 ± 4.31 a	0.15 ± 0.02 a	380.72 ± 73.83 ab
HC-LZn	61.44 ± 5.94 ab	0.17 ± 0.01 a	371.22 ± 26.11 ab
HC-MZn	76.02 ± 5.66 bc	0.16 ± 0.01 a	488.98 ± 33.23 a
HC-HZn	57.15 ± 3.26 a	0.16 ± 0.01 a	357.62 ± 1.11 b

Data are the means ± SD (n = 3). Different letters represent the significant difference ($p < 0.05$) among the Zn concentrations at the same CO_2 concentration

differences were observed in the $rETR_{max}$ values between ambient and high CO_2 levels at constant Zn level ($p > 0.05$). In addition, Zn and CO_2 exerted no interactive effect on α (p = 0.297) (Table S2). Elevated Zn concentrations did not significantly affect α under ambient and high CO_2 concentrations ($p > 0.05$) (Table S2). Furthermore, Zn and CO_2 exerted no interactive effect on I_k (p = 0.769), while the tested Zn concentrations exerted a significant effect (p = 0.001) (Table S2). Under ambient CO_2 concentration, elevated Zn concentration did not lead to a significant difference of I_k ($p > 0.05$). However, under the high CO_2 level, MZn increased I_k by 31.72% compared to that at LZn (p = 0.001), and HZn decreased I_k from 371.22 ± 26.11 to 357.62 ± 1.11 μmol photons m^{-2} s^{-1} (p = 0.782).

Effective quantum yield

Two-way ANOVA results showed that CO_2 and Zn exerted no significant interactive effect on the effective quantum yield (p = 0.505), while both CO_2 and Zn affected the effective quantum yield of *P. yezoensis* (p = 0.006 and $p < 0.001$, respectively) (Table S3). Increasing Zn concentrations did not significantly change the effective quantum yield of thalli at ambient CO_2 levels ($p > 0.05$) (Fig. 3), while the yield significantly increased from 0.36 ±0.01 (control) to 0.39 ± 0.01 (MZn) (p = 0.004) and 0.38 ± 0.01 (HZn) (p = 0.024) at high CO_2 concentrations. No significant differences were found between ambient and high CO_2 levels at different Zn concentrations ($p > 0.05$) (Fig. 3).

Photosynthetic rate

Two-way ANOVA results showed that CO_2 and Zn had a significant interaction ($p < 0.001$), where both CO_2 and Zn exerted main effects on the net photosynthetic rate of *P. yezoensis* ($p < 0.001$ and p = 0.004, respectively) (Fig. 4a, Table S4). Under ambient CO_2 concentrations, an increase in Zn concentration caused a significant decrease of the net photosynthetic rate from 235.76 ± 1.54 μmol O_2 g FW^{-1} h^{-1} (LZn) to 172.64 ± 6.55 μmol O_2 g FW^{-1} h^{-1} (MZn) (p = 0.000) and 168.90 ± 2.56 μmol O_2 g FW^{-1} h^{-1} (HZn) (p = 0.000), respectively. In contrast, high CO_2 levels increased the net photosynthetic rate from 202.12 ± 6.56 μmol O_2 g FW^{-1} h^{-1} (LZn) to 243.82 ± 14.55 μmol O_2 g FW^{-1} h^{-1} (MZn) (p = 0.007) and 222.06 ± 15.12 μmol O_2 g FW^{-1} h^{-1} (HZn) (p = 0.103), respectively (Fig. 4a). The high CO_2 concentration significantly increased the net photosynthetic rate by 41.23% (p = 0.002) and 31.47% (p = 0.004) at MZn and HZn, respectively, compared to ambient CO_2 concentration. CO_2 and Zn had a significant interactive effect on respiration ($p < 0.001$), and each had main effects ($p < 0.001$) (Fig. 4b, Table S3). The respiration rate in the MZn treatment (101.33 ± 1.17 μmol O_2 g FW^{-1} h^{-1}) was significantly higher than in the LZn treatment (83.31 ± 2.71 μmol O_2 g FW^{-1} h^{-1}) (p = 0.000), and significantly decreased to 68.52 ± 2.35 μmol O_2 g FW^{-1} h^{-1} in

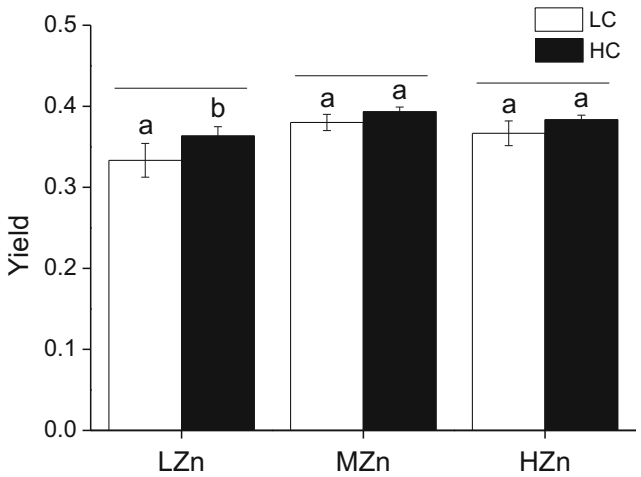

Fig. 3 Effective quantum yield of *P. yezoensis* cultured under different Zn and CO_2 concentrations. LZn, control; MZn, 25 μg L^{-1} Zn; HZn, 100 μg L^{-1} Zn; LC, 400 μatm CO_2; HC, 1000 μatm CO_2. Error bars indicate the standard deviation (n = 3). Horizontal lines represent the significant differences ($p < 0.05$) between ambient and elevated CO_2 levels at the same Zn concentrations. Different letters represent significant differences ($p < 0.05$) between different Zn concentrations at the same CO_2 concentration

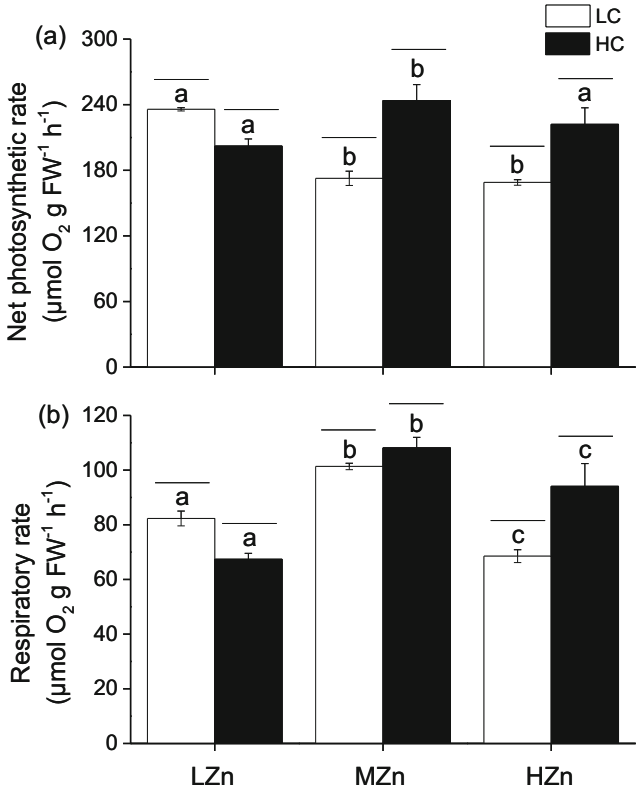

Fig. 4 Net photosynthetic rate (**a**) and respiratory rate (**b**) of *P. yezoensis* cultured under different Zn and CO_2 concentrations. LZn, control; MZn, 25 μg L^{-1} Zn; HZn, 100 μg L^{-1} Zn; LC, 400 μatm CO_2; HC, 1000 μatm CO_2. Error bars indicate the standard deviation ($n = 3$). Horizontal lines represent significant differences ($p < 0.05$) between ambient and elevated CO_2 levels at the same Zn concentration. Different letters represent significant differences ($p < 0.05$) between different Zn concentrations at the same CO_2 concentration

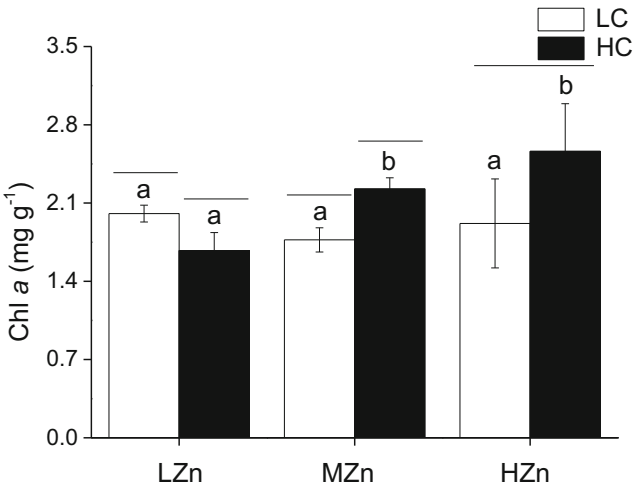

Fig. 5 The Chl *a* concentration of *P. yezoensis* grown under different Zn and CO_2 concentration conditions. LZn, control; MZn, 25 μg L^{-1} Zn; HZn, 100 μg L^{-1} Zn; LC, 400 μatm CO_2; HC, 1000 μatm CO_2. Error bars indicate the standard deviation ($n = 3$). Horizontal lines represent the significant differences ($p < 0.05$) between ambient and elevated CO_2 levels at the same Zn concentration. Different letters represent the significant differences ($p < 0.05$) between different Zn concentrations at the same CO_2 concentration

the HZn treatment at ambient CO_2 concentrations ($p = 0.000$) (Fig. 4b). A similar trend was also observed under high CO_2 concentrations, where the respiration rate increased from 67.37 ± 2.19 μmol O_2 g FW^{-1} h^{-1} in the LZn treatment to 108.14 ± 3.84 μmol O_2 g FW^{-1} h^{-1} in the MZn treatment ($p = 0.000$). The respiration significantly decreased to 94.07 ± 8.32 μmol O_2 g FW^{-1} h^{-1} in the HZn treatment ($p = 0.019$).

Chl *a*

CO_2 and Zn had a significant interaction on Chl *a* ($p = 0.008$), but neither had a dominant effect ($p = 0.078$ and $p = 0.082$, respectively), as indicated by the results of two-way ANOVA analysis (Fig. 5, Table S5). Under high CO_2 levels, the Chl *a* content of *P. yezoensis* increased by 25.96% and 32.13% in MZn and HZn treatments, respectively, compared to LZn ($p = 0.046$ and $p = 0.07$, respectively) (Fig. 5). No significant differences were found in the Chl *a* content of *P. yezoensis* at either Zn concentration, under ambient CO_2 concentrations ($p > 0.05$).

MDA content and SOD activity

CO_2 and Zn exerted no interactive effects on the MDA content of *P. yezoensis* ($p = 0.114$), while individually, both high CO_2 and high Zn conditions altered MDA concentrations ($p < 0.001$ and $p < 0.001$, respectively) (Fig. 6a, Table S6). Under ambient CO_2 concentrations, with increasing Zn levels, the MDA contents increased by 21.79% and 16.24% at MZn and HZn, respectively, compared to that at LZn ($p < 0.001$ and $p = 0.001$, respectively). At the high CO_2 concentration, elevated Zn levels significantly increased the MDA content from 18.85 ± 0.79 mmol g^{-1}(LZn) to 26.67 ± 1.13 mmol g^{-1} (MZn) ($p = 0.01$) and 22.85 ± 1.95 mmol g^{-1} (HZn) ($p = 0.33$), respectively. No significant differences were found for the MDA content between ambient and high CO_2 concentrations at MZn and HZn ($p = 0.009$ and $p = 0.008$, respectively). CO_2 and Zn exerted a significant interactive effect and both CO_2 and Zn exerted main effects on SOD activity ($p < 0.001$) (Table S6 and Fig. 6b). One-way ANOVA results showed that under ambient CO_2 conditions and with increasing Zn concentrations, SOD activity decreased significantly to 469.35 ± 16.15 U g^{-1} (MZn) ($p = 0.002$) and 319.89 ± 20.17 U g^{-1} (HZn) ($p = 0.000$), respectively, compared to control (LZn). In contrast, SOD activity was not significantly altered at different Zn levels under high CO_2 concentrations ($p > 0.05$). SOD activity significantly increased by 43.56% at HZn under high CO_2 concentration compared to ambient CO_2 concentration ($p = 0.01$) (Fig. 6).

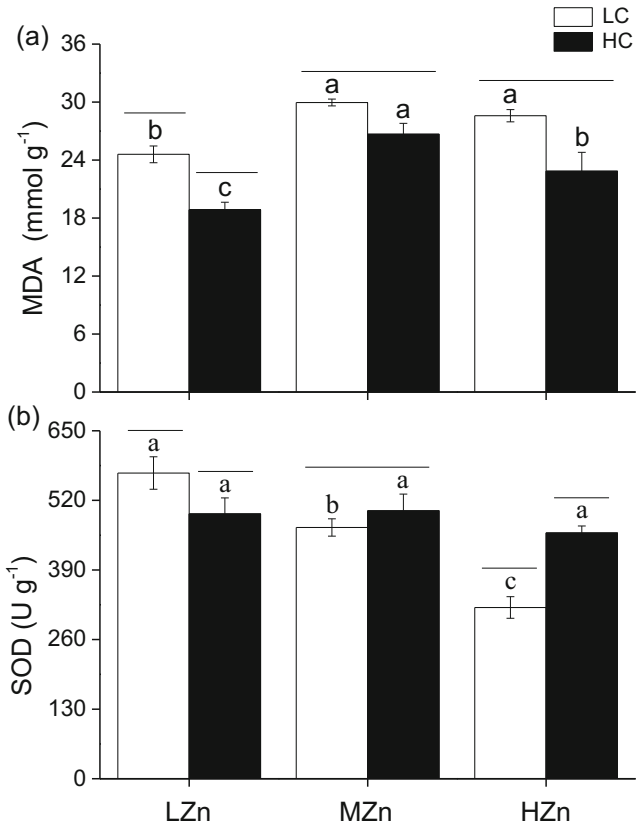

Fig. 6 MDA concentration (**a**) and SOD activity (**b**) of *P. yezoensis* cultured under different Zn and CO_2 concentrations. LZn, control; MZn, 25 μg L^{-1} Zn; HZn, 100 μg L^{-1} Zn; LC, 400 μatm CO_2; HC, 1000 μatm CO_2. Error bars indicate the standard deviation (n = 3). Horizontal lines represent significant differences ($p < 0.05$) between ambient and elevated CO_2 levels at the same Zn concentration. Different letters represent significant differences ($p < 0.05$) between different Zn levels at the same CO_2 concentration

PSII protein concentrations

The concentrations of key PSII proteins (PsbA (D1), PsbD (D2), PsbB (CP47), and RbcL) were quantified at different Zn concentrations under both ambient and high CO_2 conditions (Fig. 7). In response to ambient CO_2 conditions, D1 concentrations significantly increased in the MZn and HZn treatments compared to control. In response to high CO_2 concentrations, D1 levels significantly increased in the MZn treatment, but no significant change of the D1 concentration was observed in the HZn treatment compared to LZn. Under high CO_2 concentrations and with increasing Zn concentrations, no significant differences were observed for D2 levels. However, under ambient CO_2 levels, the D2 concentration significantly increased in the MZn treatment and decreased in the HZn treatment, compared to the LZn control. The concentration of CP47 increased with increasing Zn levels, under both ambient and high CO_2 concentrations. The concentration of RbcL decreased with increasing Zn concentrations under high CO_2 conditions. In contrast, at ambient CO_2

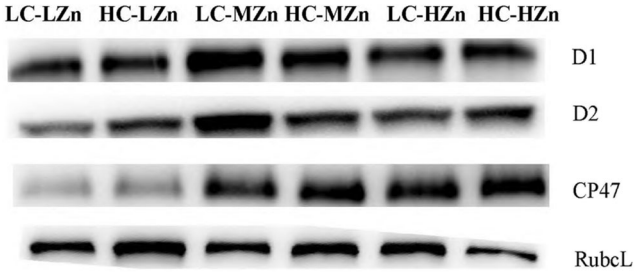

Fig. 7 Immunoblot using antibodies against photosynthesis-associated proteins of thylakoids isolated from *P. yezoensis* cultured at different Zn and CO_2 concentrations. LZn, control; MZn, 25 μg L^{-1} Zn; HZn, 100 μg L^{-1} Zn; LC, 400 μatm CO_2; HC, 1000 μatm CO_2. Each line was loaded with similar amounts of proteins. Three triplicates were conducted per treatment

levels, the RbcL concentration increased only marginally following MZn and HZn treatments.

Discussion

The obtained findings showed that the RGR of *P. yezoensis* significantly decreased under MZn and HZn treatments at same CO_2 concentration (Fig. 2). However, the significant increase in RGR of thalli in response to Zn treatment at high CO_2 concentration compared with that at ambient CO_2 concentration indicated that high CO_2 levels increased the synthesis of metal chelates, and also we hypothesis that numbers of ligand production, thus decreasing the toxic effects of this heavy metal to thalli (Gao et al. 2017). Toxic heavy metal ions can be removed from the cytoplasm via various methods, such as biochelation, precipitation, and adsorption (Moreno-Garrido et al. 1998; Zeng et al. 2015).

Photosynthesis is the sum of a series of complex metabolic reactions, the basis for the survival of the biological world, and an important medium for the carbon and oxygen cycle of the Earth (Ma et al. 2016). The negative effect on the photosynthesis was observed with the increased of Zn levels. The reduced Chl *a* content under MZn and HZn compared with LZn under the ambient CO_2 level indicated that the cell membrane was severely damaged under Zn stress (Zeng et al. 2015). A similar phenomenon was also reported for the rate of *P. yezoensis* photosynthesis, where higher Zn concentrations decreased the net photosynthetic rate of *P. yezoensis* under low CO_2 conditions, despite the increase of rETR. This suggested that more electrons were transferred to O_2 to form superoxide anions, and inhibited the photosynthesis process (Ohkubo et al. 2006). The CCMs are core metabolic mechanisms that determine the photosynthetic carbon fixation rate and in turn influence the growth of *P. yezoensis* (Li et al. 2016). It has been reported that elevated CO_2 concentrations can result in energy savings associated with the down-regulation of CCMs, thus improving the algal performance under resource limiting conditions (Gao et al. 2012; Gao et al. 2017; Qu et al. 2017), which also benefits biosynthesis and metabolism

pathways (Xu et al. 2017; Gao et al. 2018a, 2018b). The enhanced net photosynthetic rate and respiratory rate at LZn and HZn under high CO_2 concentration evidenced this results (Figs. 4 and 5). Chl *a* synthesis was also increased at that condition, which could be due to it could exchange intercellular divalent metal ions (e.g., Zn) with the Mg in Chl *a* to alleviate the toxicity of heavy metals (Chojnacka et al. 2005; Gao et al. 2017).

Plant cell membranes are often considered a primary target for heavy metal toxicity, and increased oxidative stress was demonstrated to be one of the main responses to heavy metal exposure (Xu and Gao 2012). In the present study, MDA concentrations significantly increased when thalli were exposed to Zn, compared to the control under ambient CO_2 concentrations (Fig. 6a). These findings suggest that increased Zn levels indirectly resulted in ROS overproduction, enhanced lipid peroxidation, and consequently, induced oxidative stress in algae (Soto 2011; Alharby et al. 2016). These results are in accordance with a prior study on the green algae *Pseudokirchneriella subcapitata* in response to Zn exposure (Soto 2011). Plants can activate protective mechanisms to scavenge ROS (Singh et al. 2006), which are important for the prevention of plant oxidative stress by increasing the activity of one or more enzymes in response to Zn stress (Yang et al. 2016). SOD is a primary antioxidant, which converts the superoxide radical ($O_2^{\cdot-}$) to H_2O_2 and can be used to indicate antioxidative defenses (Rijstenbil 2001; Chelikani et al. 2004). In the present study, Zn stress resulted in a significant decrease in SOD activity under ambient CO_2 levels. However, no significant change in SOD activity was observed with increasing Zn concentrations in response to high CO_2 conditions (Fig. 6b). This result can be attributed to the enhanced defense capacity of thalli under elevated CO_2 levels, which removed excess H_2O_2 and prevented cellular damage (Yuan et al. 2018).

Abiotic stressors, such as exposure to heavy metals and ocean acidification can affect plants by altering their protein contents (Yang et al. 2011). Under high CO_2 conditions, the concentration of the D1 protein decreased in response to MZn treatment, which may be due to the light-induced phosphorylation of PSII. Particularly, the D1 protein has been reported to be easily photodamaged during the photosynthetic light reaction (Takahashi et al. 2007). The damaged D1 protein is rapidly degraded and synthesized de novo, and the new D1 protein is then inserted into the PSII (Zhang and Aro 2002). The D1 protein concentration increased under high CO_2 conditions, suggesting that ocean acidification promotes the turnover of D1 proteins, thus alleviating the photooxidation of heavy metals on thalli. The increases of RGR, net photosynthetic, and respiratory rate further corroborate this hypothesis. The D2 protein subunit of the PSII reaction center is encoded by *psbD* and is the rate-determining step for the PSII assembly (Asada et al. 2018). The D2 protein concentration increased in this study, in response to increasing Zn concentrations, suggesting that PSII activity was stimulated. The chlorophyll-binding protein CP47 (PsbB) is encoded by the *psbB* gene, together with the chlorophyll-binding protein CP43. CP43 is also located in algal membranes, where it is assembled in the inner light-harvesting complex (Clarke and Eaton-Rye 2000; De Weerd et al. 2013) and serves as the core antenna of the PS II. CP47 concentrations were also elevated by increased Zn concentrations, especially in response to high CO_2 levels (Fig. 7). This may be attributed to the excess energy generated by the transfer of outer light-harvesting complexes to the PsbA/PsbD heterodimer (Pospíšil 2014).

Conclusions

This study investigated the photosynthetic physiological and biochemical changes of *P. yezoensis* grown in the presence of different Zn concentrations, and under conditions that simulate both current and future ocean acidification. The obtained findings indicate that elevated Zn concentrations decreased the algal relative growth rate, effective quantum yield, net photosynthetic rate, and respiratory rate. SOD activity was also stimulated to increase the removal of the large amount of superoxide anions generated by Zn stress, and thus offset the damage to the cell membrane caused by heavy metal exposure (Pandey et al. 2009). Further studies with other seaweed species are required to better understand the interaction between ocean acidification and Zn pollution and how this affects the seaweed community. Furthermore, other heavy metals should be assessed to obtain a more comprehensive view of the combined effects of climate change and heavy metal pollution.

Funding information This study was supported by the Natural Science Foundation of Jiangsu Province (Nos. BK20181075 and BK20161295), Modern Fisheries Industrial Research System of Jiangsu Province (JFRS-04), the Postdoctoral Science Foundation of Jiangsu Province, Open-end Funds of Jiangsu Key Laboratory of Marine Biotechnology, Huaihai Institute of Technology (No. HS2018005), the Science Foundation of Huaihai Institute of Technology (No. Z2017009), the China Postdoctoral Science Foundation (Nos. 2019M651431, 2018T110463, and 2017M620270), Postgraduate research & Practice Innovation Program of Jiangsu Province and the Priority Academic Program Development of Jiangsu Higher Education Institutions and the Excellent Undergraduate Thesis (Design) Training Program of Huaihai Institute of Technology (No. 5501006).

References

Alharby HF, Metwali EMR, Fuller MP, Aldhebiani AY (2016) Impact of application of zinc oxide nanoparticles on callus induction, plant regeneration, element content and antioxidant enzyme activity in tomato (*Solanum lycopersicum* Mill.) under salt stress. Arch Biol Sci 68:723–735

Asada M, Nishimura T, Ifuku K, Mino H (2018) Location of the extrinsic subunit psbp in photosystem II studied by pulsed electron-electron double resonance. Biochim Biophys Acta 1859:394–399

Boyer GL, Brand LE (1998) Trace elements and harmful algal blooms. Nato Asi Ser G 41:489–508

Branzini A, González RS, Zubillaga M (2012) Absorption and translocation of copper, zinc and chromium by *Sesbania virgata*. J Environ Manag 102:50–54

Brierley AS, Kingsford MJ (2009) Impacts of climate change on marine organisms and ecosystems. Curr Biol 19:602–614

Cai WJ, Hu X, Huang WJ, Murrell MC, Lehrter JC, Lohrenz SE, Chou WC, Zhai W, Hollibaugh JT, Wang Y (2011) Acidification of subsurface coastal waters enhanced by eutrophication. Nat Geosci 4: 766–770

Cai ZP, Liu WJ, Duan SS (2019) Growth and physiological response of *Karenia mikimotoi* to heavy metal Zn^{2+} stress. Ecol Sci 38:176–181

Caldeira K, Wickett ME (2003) Anthropogenic carbon and ocean pH. Nature 425:365

Chakraborty S, Owens G (2015) Erratum to: Metal distributions in seawater, sediment and marine benthic macroalgae from the South Australian coastline. Int J Environ Sci Technol 12:1479–1480

Chelikani P, Fita I, Loewen PC (2004) Diversity of structures and properties among catalases. Cell Mol Life Sci 61:192–208

Chojnacka K, Chojnacki A, Gorecka H (2005) Biosorption of Cr^{3+}, Cd^{2+} and Cu^{2+} ions by blue-green algae Spirulina sp.: kinetics, equilibrium and the mechanism of the process. Chemosphere 59:75–84

Clark KD, Costen PG, Fowler GD, Lockwood FC, Yousif S (2002) The influence of combustion configuration and fuel type on heavy-metal emissions from a pulverized-fuel-fired combustor. Proc Combust Inst 29:433–440

Clarke SM, Eaton-Rye JJ (2000) Amino acid deletions in loop C of the chlorophyll a-binding protein CP47 alter the chloride requirement and/or prevent the assembly of photosystem II. Plant Mol Biol 44: 591–601

Cornwall CE, Hepburn CD, Pritchard D, Curri KI, Mcgraw CM, Hunter KA, Hurd CL (2012) Carbon-use strategies in macroalgae: differential responses to lowered ph and implications for ocean acidification. J Phycol 48:137–144

De Weerd FL, Palacios MA, Andrizhiyevskaya EG, Dekker JP, Van GR (2013) Identifying the lowest electronic states of the chlorophylls in the CP47 core antenna protein of photosystem II. Biochemistry 41: 15224–15233

Doney S (2009) The consequences of human-driven ocean acidification for marine life. F1000 Biol Rep 1:36–40

Eilers PHC, Peeters JCH (1988) A model for the relationship between light intensity and the rate of photosynthesis in phytoplankton. Ecol Model 42:199–215

Franklin NM, Stauber JL, Markich SJ, Lim RP (2000) pH-dependent toxicity of copper and uranium to a tropical freshwater alga (*Chlorella sp.*). Aquat Toxicol 48:275–289

Gao KS, Aruga Y, Asada K, Ishihara T, Akano T, Kiyohara M (1991) Enhanced growth of the red alga Porphyra yezoensis ueda in high CO_2 concentrations. J Appl Phycol 3:355–362

Gao G, Gao K, Giordano M (2009) Responses to solar UV radiation of the diatom *Skeletonema costatum* (bacillariophyceae) grown at different Zn^{2+} concentrations. J Phycol 45:119–129

Gao KS, Xu JT, Gao G, Li YH, Hutchins DA, Huang BQ, Wang L, Zheng Y, Jin P, Cai XN, Donat-Peter H, Li W, Xu K, Liu NN, Ulf R (2012) Rising CO_2 and increased light exposure synergistically reduce marine primary productivity. Nat Clim Chang 2:519–523

Gao G, Liu YM, Li XS, Feng ZH, Xu ZG, Wu HY, Xu JT (2017) Expected CO_2-induced ocean acidification modulates copper toxicity in the green tide alga *Ulva prolifera*. Environ Exp Bot 135:63–72

Gao G, Clare AS, Rose C, Caldwell GS (2018a) *Ulva rigida* in the future ocean: potential for carbon capture, bioremediation, and biomethane production. GCB Bioenergy 10:39–51

Gao G, Shi Q, Xu Z, Xu JT, Campbell DA, Wu H (2018b) Global warming interacts with ocean acidification to alter PSII function and protection in the diatom *Thalassiosira weissflogii*. Environ Exp Bot 147:95–103

Gao G, Gao Q, Bao ML, Xu J, Li X (2019) Nitrogen availability modulates the effects of ocean acidification on biomass yield and food quality of a marine crop *Pyropia yezoensis*. Food Chem 271:623–629

García-Sánchez MJ, Fernandez JA, Niell X (1994) Effect of inorganic carbon supply on the photosynthetic physiology of *Gracilaria tenuistipitata*. Planta 194:55–61

Gattuso JP, Payri CE, Pichon M, Delesalle B, Frankignoulle M (1997) Primary production, calcification, and air-sea CO_2 fluxes of macroalgal-dominated coral reef community (Moorea, French Polynesia). J Phycol 33:729–738

Gattuso JP, Magnan A, Billé R, Cheung WW, Howes EL, Joos F, Allemand D, Bopp L, Cooley SR, Eakin CM, Hoegh-Guldberg O (2015) Contrasting futures for ocean and society from different anthropogenic CO_2 emissions scenarios. Science 349:aac4722

Genty B, Briantais JM, Baker NR (1989) The relationship between the quantum yield of photosynthetic electron transport and quenching of chlorophyll fluorescence. BBA- Gen Subj 990:87–92

Haglund K, Björklund M, Gunnare S, Sandberg A, Olander U, Pedersén M (1996) New method for toxicity assessment in marine and brackish environments using the macroalga *Gracilaria tenuistipitata* (Gracilariales, Rhodophyta). Hydrobiologia 326–327:317–325

Hepburn CD, Pritchard DW, Cornwall CE, Mcleod RJ, Beardall J, Raven JA, Hued CL (2011) Diversity of carbon use strategies in a kelp forest community: implications for a high CO_2 ocean. Glob Chang Biol 17:2488–2497

Jiang YZ, Prognon P (2006) Raw material enzymatic activity determination: A specific case for validation and comparison of analytical methods -The example of superoxide dismutase (SOD). J Pharm Biomed Anal 40:1143–1148

Kuffner IB, Andersson AJ, Jokiel PL, Ku'ulei SR, Mackenzie FT (2008) Decreased abundance of crustose coralline algae due to ocean acidification. Nat Geosci 1:114–117

Landschützer P, Gruber N, Bakker DCE, Stemmler I, Six KD (2018) Strengthening seasonal marine CO_2 variations due to increasing atmospheric CO_2. Nat Clim Chang 8:146–150

Leal PP, Hurd CL, Sander SG, Armstrong E, Roleda MY (2016) Copper ecotoxicology of marine algae: a methodological appraisal. Chem Ecol 32:786–800

Leal PP, Hurd CL, Sander SG, Armstrong E, Fernández PA, Suhrhoff TJ, Roleda MY (2018) Copper pollution exacerbates the effects of ocean acidification and warming on kelp microscopic early life stages. Sci Rep-UK 8:147163–147176

Leclercq N, Gattuso JP, Jaubert J (2002) Primary production, respiration, and calcification of a coral reef mesocosm under increased CO_2 partial pressure. Limnol Oceanogr 47:558–564

Leusch A, Holan ZR, Volesky B (1995) Biosorption of heavy metals (Cd, Cu, Ni, Pb, Zn) by chemically-reinforced biomass of marine algae. J Chem Technol Biotechnol 62:279–288

Li XS, Xu JT, He PM (2016) Comparative research on inorganic carbon acquisition by the macroalgae *Ulva prolifera* (Chlorophyta) and *Pyropia yezoensis* (Rhodophyta). J Appl Phycol 28:491–497

Lv F, Ding G, Wu HY, Li MZ (2017) Comparative study on heavy metal accumulation in *Sargassum muticum* and *Gracilaria chouae*. Mar Sci 41:18–23

Ma JH, Cai SQ (1996) Cultivation and process of Porphyra yezoensis. Sci, Beijing, 12–13, in Chinese

Ma J, Lv CF, Xu ML, Chen GX, Lv CG, Gao ZP (2016) Photosynthesis performance, antioxidant enzymes, and ultrastructural analyses of rice seedlings under chromium stress. Environ Sci Pollut Res Int 23:1768–1778

Macedo MF, Duarte P, Ferreira JG (2002) The influence of incubation periods on photosynthesis-irradiance curves. J Exp Mar Biol Ecol 274:101–120

Mallick S, Sinam G, Mishra RK, Sinha S (2010) Interactive effects of Cr and Fe treatments on plants growth, nutrition and oxidative status in *Zea mays* L. Ecotoxicol Environ Saf 73:987–995

Mamboya F, Lyimo TJ, Landberg T, Björk M (2009) Influence of combined changes in salinity and copper modulation on growth and copper uptake in the tropical green macroalga *Ulva reticulata*. Estuar Coast Shelf Sci 84:326–330

MillerO FNJ, Woosley R, Ditrolio B, Waters J (2009) Effect of ocean acidification on the speciation of metals in seawater. Oceanography 22:72–85

Moreno-Garrido I, Blasco J, Gonzalez-Delvalle M, Lubian LM (1998) Differences in copper accumulation by the marine microalga Nannochloropsis gaditana Lubian, submitted to two different thermal treatments. Ecotox Environ Restor 1:43–47

Mousavi SR, Galavi M, Rezaei M (2012) The interaction of zinc with other elements in plants: a review. Int J Agricult Crop Sci 4:1881–1884

Nanda R, Agrawal V (2016) Elucidation of zinc and copper induced oxidative stress: DNA damage and activation of defence system during seed germination in Cassia angustifolia Vahl. Environ Exp Bot 125:31–41

Ohkubo K, Kitaguchi H, Fukuzumi S (2006) Activation of electron-transfer reduction of oxygen by hydrogen bond formation of superoxide anion with ammonium ion. J Phys Chem A 110:11613–11616

Omar HH (2002) Bioremoval of zinc ions by *Scenedesmus obliquus* and *Scenedesmus quadricauda* and its effect on growth and metabolism. Int Biodeterior Biodegrad 50:95–100

Pandey N, Pathak GC, Pandey DK, Pandey R (2009) Heavy metals, Co, Ni, Cu, Zn and Cd, produce oxidative damage and evoke differential antioxidant responses in spinach. Braz J Plant Physiol 21:103–111

Porra RJ, Thompson WA, Kriedemann PE (1989) Determination of accurate extinction coefficients and simultaneous equations for assaying chlorophylls a, and b, extracted with four different solvents: verification of the concentration of chlorophyll standards by atomic absorption spectroscopy. BBA-Bioenergetics 975:384–394

Pospíšil P (2014) The role of metals in production and scavenging of reactive oxygen species in photosystem II. Plant Cell Physiol 55: 1224–1232

Qu LM, Xu JT, Sun JZ, Li XS, Gao KS (2017) Diurnal pH fluctuations of seawater influence the responses of an economic red macroalga *Gracilaria lemaneiformis* to future CO_2 -induced seawater acidification. Aquaculture 473:383–388

Rijstenbil JW (2001) Effects of periodic, low UVA radiation on cell characteristics and oxidative stress in the marine planktonic diatom *Ditylum brightwellii*. Eur J Phycol 36:1–8

Sadiq IM, Dalai S, Chandrasekaran N, Mukherjee A (2011) Ecotoxicity study of titania (TiO_2) NPs on two microalgae species: *Scenedesmus* sp. and *Chlorella* sp. Ecotoxicol Environ Saf 74:1180–1187

Singh S, Eapen S, D'Souza SF (2006) Cadmium accumulation and its influence on lipid peroxidation and antioxidative system in an aquatic plant *Bacopa monnieri* L. Chemosphere 62:233–246

Soto P (2011) Assessment of catalase activity, lipid peroxidation, chlorophyll-a, and growth rate in the freshwater green algae *Pseudokirchneriella subcapitata* exposed to copper and zinc. Lat Am J Aquat Res 39:280–285

Stewart J, Tolliver R, Field DB, Young C, Stafford G, Day RD (2016) Multi-decadal records of ocean acidification and toxic heavy metal pollution in coral cores from Oahu, Hawaii. AGU Fall Meeting Abstracts

Stoneman A, Smith S (2012) Effects of ocean acidification on otolith growth of the mummichog. American Fisheries Society 1 Meeting

Takahashi S, Bauwe H, Badger M (2007) Impairment of the photorespiratory pathway accelerates photoinhibition of photosystem II by suppression of repair but not acceleration of damage processes in Arabidopsis. Plant Physiol 144:487–494

Volland S, Bayer E, Baumgartner V, Andosch A, Lütz C, Sima E, Lütz-Meind U (2014) Rescue of heavy metal effects on cell physiology of the algal model system *Micrasterias* by divalent ions. J Plant Physiol 171:154–163

Webster NS, Uthicke S, Botté ES, Flores F, Negri AP (2013) Ocean acidification reduces induction of coral settlement by crustose coralline algae. Glob Chang Biol 19:303–315

Xu JT, Gao KS (2012) Future CO_2-induced ocean acidification mediates the physiological performance of a green tide alga. Plant Physiol 160:1762–1769

Xu ZG, Gao G, Xu JT, Wu HY (2017) Physiological response of a golden tide alga (*Sargassum muticum*) to the interaction of ocean acidification and phosphorus enrichment. Biogeosciences 14:671–681

Yang YL, Zhang YY, Wei XL, You J, Wang WR, Lu J, Shi RX (2011) Comparative antioxidative responses and proline metabolism in two wheat cultivars under short term lead stress. Ecotoxicol Environ Saf 74:733–740

Yang YL, Ma T, Ding F, Ma HZ, Duan XH, Gao TP, Yao J (2016) Interactive zinc, iron, and copper-induced phytotoxicity in wheat roots. Environ Sci Pollut Res Int 24:395–404

Yuan WB, Gao G, Shi Q, Xu ZG, Wu HY (2018) Combined effects of ocean acidification and warming on physiological response of the diatom *thalassiosira pseudonana* to light challenges. Mar Environ Res 135:63–69

Zeng X, Chen X, Zhuang J (2015) The positive relationship between ocean acidification and pollution. Mar Pollut Bull 91:14–21

Zhang L, Aro EM (2002) Synthesis, membrane insertion and assembly of the chloroplast-encoded D1 protein into photosystem II. FEBS Lett 512:13–18

Zou D, Gao K (2005) Ecophysiological characteristics of four intertidal marine macroalgae during emersion along Shantou coast of China, with a special reference to the relationship of photosynthesis and CO_2. Acta Oceanol Sin 24:105–113